



Mechano-electro-magneto-optical properties of giant PCBM crystals

Scott Newacheck, Nha Uyen Huynh and George Youssef

Experimental Mechanics Laboratory, San Diego State University, San Diego, CA, USA

ABSTRACT

Millimetre-scale rhombohedral PCBM crystals were fabricated on multiple substrates, including metalised glass and polymer. The multi-substrate fabrications granted the ability of characterising the crystals composition, magnetically, electrically, and mechanically. Colossal crystals were fabricated with or without P3HT, elucidating novel capabilities of the crystals for flexible and wearable electronics applications. The lone PCBM crystals were characterised for their optical and mechanical properties, whereas the P3HT coated crystals have notable magnetic and conductive performances. The substrate type played a crucial role in property-map of this organic framework, including crystal growth and segregation. The PCBM crystals combined with P3HT hold a promising future for organic photovoltaics and magnetic systems.

ARTICLE HISTORY

Received 6 March 2024 Accepted 28 August 2024

KEYWORDS

Organic multiferroics; organic crystals; magnetoelectric; terahertz

Wearable and flexible electronics require a paradigm shift in material science and engineering. The material must exhibit high efficacy for the bidirectional conversion of magnetic and electrical energies, pointing towards oxide-based crystalline materials. However, the available materials exhibit poor mechanical flexibility and fatigue life. Multiple research directions focused on exploring metal-perovskite thin films [1], traditional extrinsic and intrinsic multiferroics [2], and metal-organic frameworks [3], to address this challenge. Recently, blends of conjugated polymers with molecular acceptors have attracted much attention in photovoltaic applications with a potential magnetoelectric response. Examples of these conjugated polymers include P3HT, MEH-PPV, MDMO-PPV, while molecular acceptors include PCBM, C_{60} , and $PC_{70}BM$ [4–6].

Poly 3-hexylthiophene-2,5-diyl (P3HT) blended with Phenyl-C₆₁-butyric acid methyl ester (PCBM) is a rigorously researched material system for organic photovoltaic (OPV) technologies, achieving nearly 5% efficiency in some cases [7,8]. The fascinating capability of this composite macromolecule could be leveraged in organic magnetoresistance (OMAR) and organic ferromagnetic technologies [9-11]. The coexistence of the P3HT and PCBM in semiconductive polymer frameworks gives rise to charge-transfer excitonics, theorised to be the source of their magnetic and magnetoresistive properties. The culmination of the electrical, mechanical, and magnetic properties in excitonic polymers situates them as a material candidate for wearable and flexible electronics. For example, P3HT:PCBM thin films exhibit 16% magnetoresistivity at a 0.3 T magnetic field, i. e., organic magnetic field sensors [12]. The same polymer framework reported a magnetic saturation of 0.65 emu/g at 0.1 T when light is applied, implying suitability for organic optomagnetic applications [13].

Most OPV, OMAR, and organic magnets have been fabricated on smooth rigid substrates, e.g., glass or silicon wafers, for their planarity and handling [6]. Glass and silicon are chemically resilient to nearly all organic solvents used to fabricate these conjugated polymers, and thermally stable to endure the stresses from thermal treatments. Moreover, these inorganic substrates are more conducive for depositing conductive and transparent layers (e.g., ITO) necessary for OPV and vertical OMAR devices. However, some research groups have successfully fabricated P3HT:PCBM OPV on polyethylene with similar efficiencies to devices fabricated on glass, demonstrating the potential for all-polymer devices [14]. The latter improves the prospects of conjugated polymers in flexible and wearable electronic applications, trumping their inorganic counterparts.

This research investigates the effect of the substrate on the mechanical, electrical, and magnetic performance of P3HT: PCBM composite by growing 'colossal' crystals on glass, glass-coated ITO, and PVDF membrane filters. Our group recently demonstrated the process of growing PCBM with sizes exceeding 1 mm, representing over a 600% increase over the state-of-the-art [15]. The exceptional crystal growth (referred to as 'colossal' hereafter) was attributed to the low surface area-to-volume ratio, causing the external layer to solidify and entrap the solvent and slowing down the curing time of the interior. The substrate selection has been shown to affect the film growth characteristics [16,17]. When P3HT: PCBM is investigated for photovoltaic application, ITOcoated glass is of primary interest as a substrate for its transparency good electrical conductance. and Alternatively, standalone PVDF is suitable for ferroelectric and piezoelectric electronic applications and has excellent mechanical and chemical resilience to withstand the fabrication process of P3HT:PCBM and loading conditions during normal deployment conditions. In the context of this research, PVDF facilitated the dynamic mechanical characterisation of P3HT:PCBM, for the first time since other substrates either dominate the response or are not conducive for lifting off the films.

Regioregular poly(3-hexylthiophene) (Rieke Metals) was dissolved entirely in ortho-dichlorobenzene (ODCB) with a concentration of 35 mg/mL. Phenyl-C₆₁-butyric acid



methyl ester (Nano-C) was then added to the solution in a 1:1 weight ratio concerning P3HT and stirred at 40°C for 15 h. The solution was drop cast onto a PVDF membrane (Durapore DVPP02500) previously ultrasound cleaned with deionised water, glass, or ITO-coated glass cleaned with isopropyl alcohol. Samples were then left in a controlled environment to cure for enhanced crystallinity. All fabrication steps were performed in an inert N_2 environment, while all characterisation steps were done in ambient conditions.

Magnetic characterisation was performed on a Quantum Design MPMS in DC mode and a dark environment. The microscale electrical characterisation was conducted using AFM workshop TT1 with Pl/Cr coated tips, while the macroscale electrical characterisation was accomplished with a Terahertz Time-Domain setup [18]. Finally, the mechanical characterisation was performed on a TA Instruments Q800 DMA in film tension mode.

Figure 1 encompasses the multiscale microscopy investigation of P3HT:PCBM crystals grown on different substrates, including bare glass, ITO-coated glass, and PVDF membrane. Regardless of the substrate type, the images in the figure demonstrate the ubiquity and 'colossal' crystal size,

where the crystal sizes range from $50 \, \mu m$ to $1300 \, \mu m$. While several researchers reported the nucleation of P3HT:PCBM crystals on silicon or ITO-coated glass, the crystal size is usually on the order of the film thickness ca. $10-80 \, \mu m$. On the contrary, the colossal crystals shown in Figure 1 grow out of the film, attributed to the long curing cycle to control the volume-to-surface area ratio.

Figure 1(a) shows an SEM micrograph of P3HT:PCBM crystals fabricated on glass, whereas Figure 1(b) focuses on a single crystal with exemplary uniformity and symmetry. On the one hand, when fabricated on solid and rigid substrates, e.g., glass, ITO-coated glass, or silicon, the crystals formed underneath a capping polymer layer of P3HT. A few smaller crystals barely protruding from the top capping layer are observed in Figure 1(a). The top capping layer was gently peeled off to uncover the crystals underneath, revealing many crystals with morphology similar to Figure 1(c). The rough surface of the exposed crystal is likely due to a strong bond with the P3HT capping layer, damaging the crystal during extraction. The strong bond between layers is beneficial for its conductivity and photovoltaic efficiency. On the other hand, fabricating these crystals on the PVDF

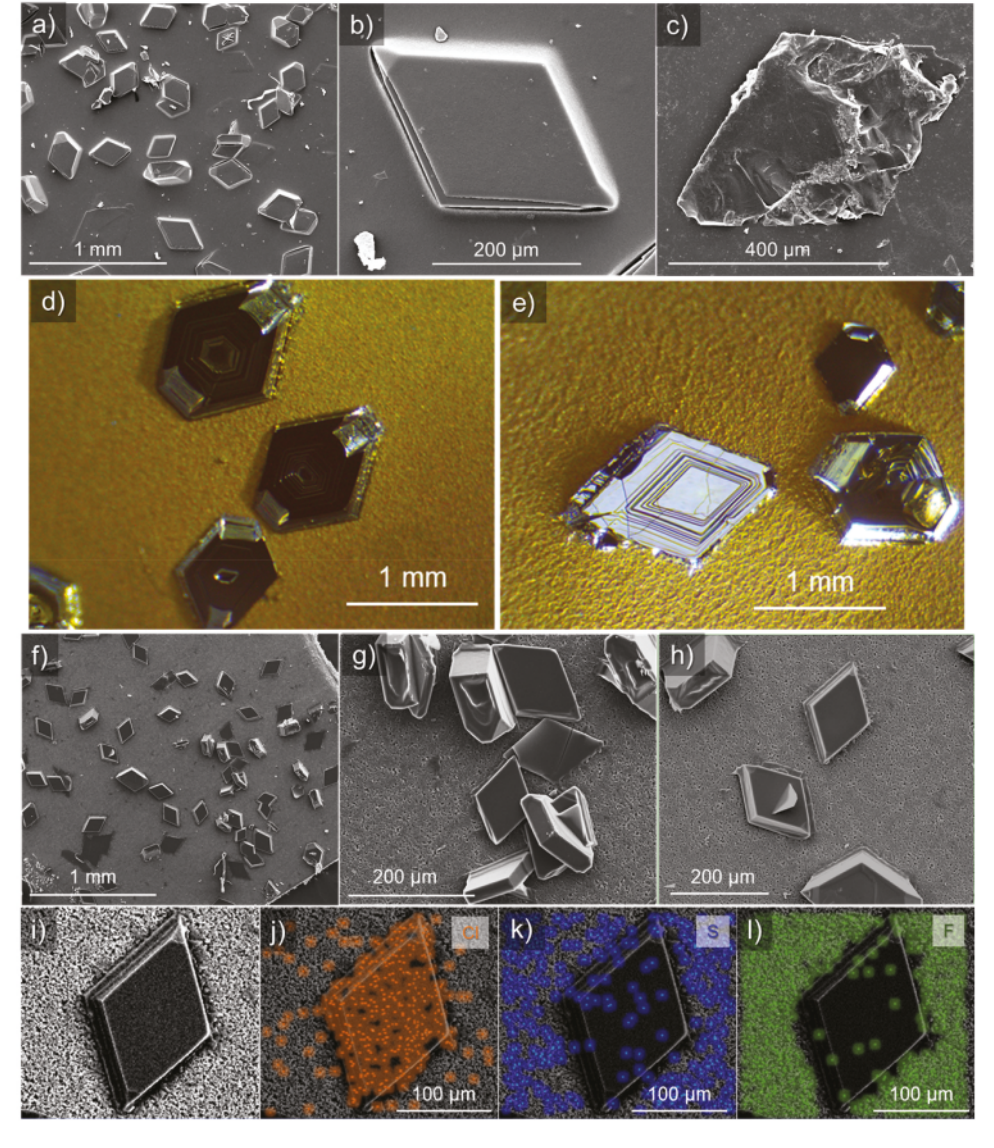


Figure 1. (a, b) SEM micrographs of P3HT:PCBM fabricated on glass substrates, (c) PCBM crystal after the P3HT layer was lifted. (d-e) a collection of P3HT:PCBM micrographs fabricated on the PVDF membrane filter, elucidating their geometrical structure. (f-h) SEM micrographs of the organic crystals demonstrating potential geometry formations. (i-l) SEM micrograph of a crystal fabricated on PVDF with superimposed EDS maps for chlorine, sulphur, and fluorine, revealing the chemical composition.

membrane exposed the PCBM formations to the top surface, as observed in the optical microscope photographs in Figure 1(d,e). It is worth noting that the PVDF membrane acted as an active separator, segregating the PCBM colossal crystals on the top from the P3HT crystals on the bottom. In some instances, several PCBM crystals were found lingering at the bottom of the PVDF membrane. This approach could grow large PCBM crystals separated from P3HT crystals for basic micro- and nano-scale characterisation. The P3HT and PCBM components partition revealed the crystal black colour owed to the fullerene derivative and smooth reflective surfaces. Moreover, the sequential layer-by-layer formation of the PCBM crystals is manifested as concentric, stepped boundaries around the perimeter.

The exposed PCBM crystals on PVDF were coated with platinum for scanning electron microscopy (shown in Figure 1d-f), which covered the feature ridges, causing a similar appearance to the P3HT-coated crystals in Figure 1a,b. Unique to the PVDF membrane substrate is the multi-directionality of the crystal growth, where Figure 1e shows an SEM micrograph exemplifying out-ofplane growth and crystal-to-crystal interactions. The bottom panel in Figure 1 shows elemental composition maps extracted from and surrounding a single PCBM crystal, where the first subpanel is an SEM micrograph of the isolated crystal, while the subsequent subpanels show the chlorine, sulphur, and fluorine concentration maps. The EDS analysis elucidates a large chlorine concentration in the PCBM crystal, while fluorine and sulphur were only present in the surrounding PVDF membrane. The elemental composition confirms our previous report that the PCBM crystals include residual dichlorobenzene solvent with a trace amount of P3HT. Fluorine or sulphur was not detected beneath the crystal due to the relatively shallow penetration depth of EDS (\sim 1 µm) compared to the crystal thickness.

The magnetic response of P3HT:PCBM as a donoracceptor organic framework hinges on the charge transfer between these two components; hence, the absence or separation of the constituents compromises their magnetic behaviour. Figure 2 provides evidence for the dependence of the magnetic response on the cohabitation of the donor and acceptor macromolecules, where the film cast on a glass substrate ensured the coexistence of the P3HT and PCBM, resulting in a ferromagnetic response. The P3HT:PCBM crystals on glass yielded a magnetic saturation of 8.2 emu/cm [3], which agrees with the previously reported 10 emu/cm [3] magnetic saturation of the same organic framework when deposited on the ITO-coated substrate. On the other hand, the film fabricated on the PVDF membrane shows a diamagnetic response since the membrane successfully segregated the two phases (e.g., Figure 1). Typically, some magnetic behaviour is observed for P3HT and PCBM as separate phases; however, the large volume fraction of diamagnetic PVDF overpowers the response. These observations affirm that the coexistence of P3HT and PCBM is essential for magnetic functionality.

The requirements for a material candidate for wearable electronics include electrical conductivity. Probing the electrical properties of the P3HT:PCBM was divided into two stages based on the substrate type. First, the crystals fabricated on ITO-coated glass were probed for microscale I-V measurements, utilising the substrate as a ground plate. Second, the samples fabricated on PVDF and glass were suitable for terahertz time-domain (THz-TD) spectroscopy in transmission mode due to the transparency of the substrates within the terahertz regime, measuring the complex electric properties [19,20].

Microscale electrical characterisation of the P3HT: PCBM crystals fabricated on ITO-coated glass were carried out using conductive atomic force microscopy (C-AFM). The conductivity maps and localised I-V curves were collected from different locations: near, on edge, and at the centre of a PCBM crystal coated with P3HT, plotted in Figure 3(a). The results also elucidate the underlying location-dependent electrical behaviour. Notably, additional current measurements were collected far away from the crystals but resulted in negligible values, hence omitted for brevity. The near-

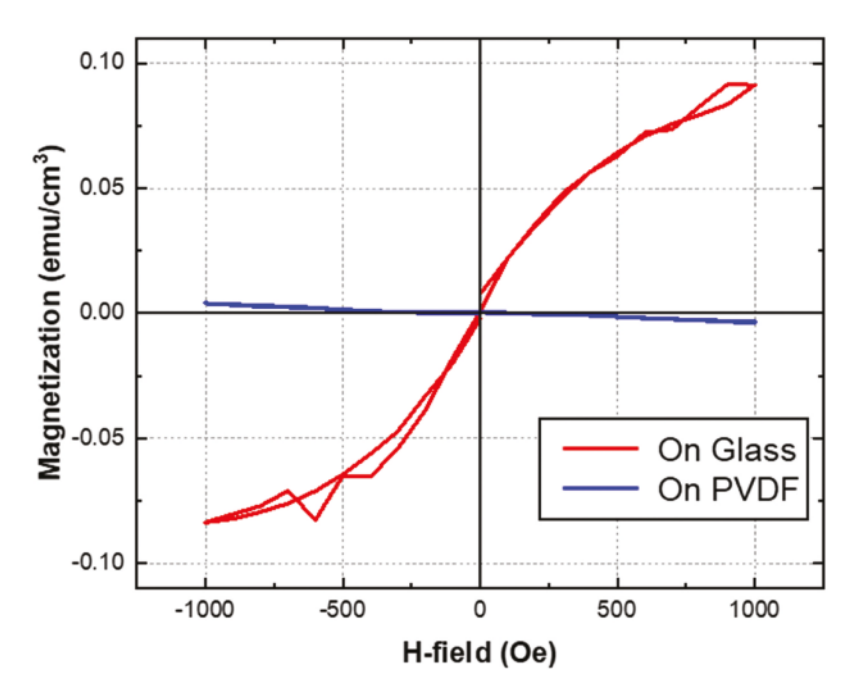


Figure 2. Magnetic hysteresis of P3HT:PCBM deposited on a glass substrate with pronounced ferromagnetic response and PVDF membrane with a diamagnetic response.

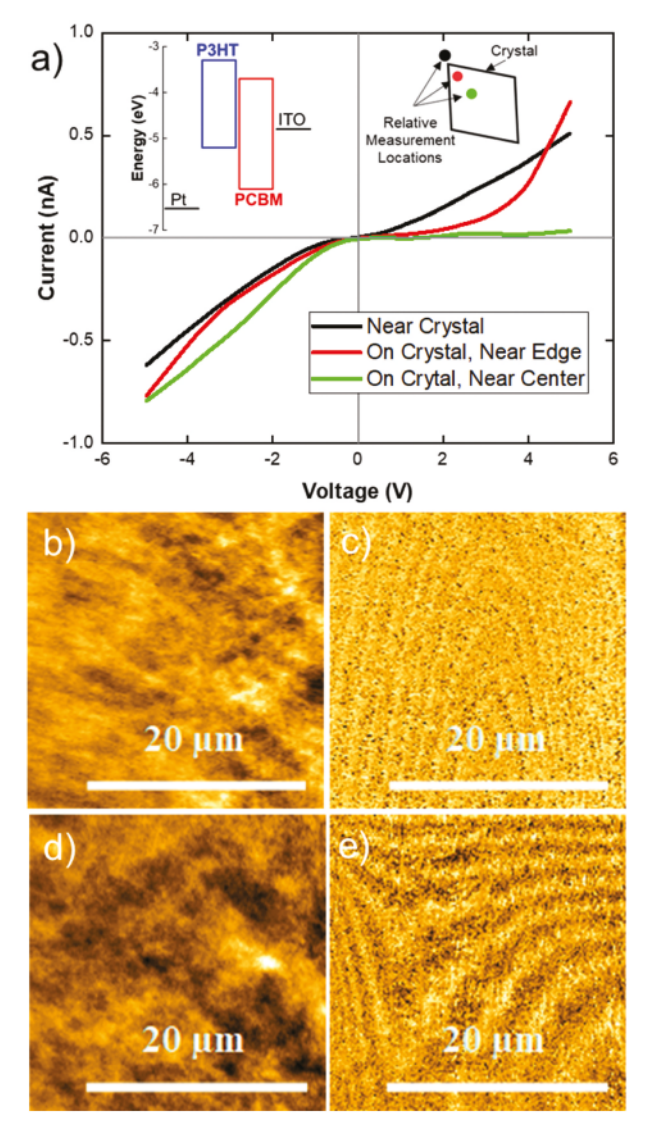


Figure 3. (a) I-V curves of P3HT:PCBM crystal on ITO-coated glass (the left inset shows the bandgap energies of P3HT, PCBM, and work functions of ITO and Pt; the right inset shows a schematic diagram of the relative locations of the measurement to a P3HT:PCBM crystal). (b-c) topography and conductive phase maps near and (d-e) on the crystal.

crystal I-V curve exhibited a semi-symmetrical, resister-like behaviour with a resistance of 7.9 G Ω . The resistance reported herein is significantly lower than prior C-AFM measurements on non-crystalline P3HT:PCBM, especially when considering the difference in thicknesses (12.5 G Ω and 50 nm thick) [21]. On the other hand, the remaining I-V curves on the crystal reported a diode-like characteristic with similar negative resistances of $6.5 \,\mathrm{G}\Omega$ and $6.4 \,\mathrm{G}\Omega$ (at -5 V). Uniquely, the I-V measured near the edge of the crystal showed a dramatic forward breakdown voltage (Vz) at 3.38 V. In contrast, the I-V curve measured near the centre of the crystal did not exhibit a breakdown voltage within the 5 V testing envelope (potential electric breakdown above 5 V). The perceived shift in breakdown voltage may be due to the increased sample thickness near the centre of the crystal since electrical breakdown is exponentially proportional to the applied electric field.

Conductive maps were measured near and on the crystal and are displayed in Figure 3b–e, respectively. The conductive phase maps near and on the crystal show a ridge pattern, closely mimicking the patterns observed in Figure 1d,e. The connection of the conductivity and optical patterns suggests

that the edges of the crystal ridges play a significant role in the conductivity, possibly due to a better interconnectedness between the material phases. This claim is substantiated by the ridges that are faintly imprinted in the topography in the near-crystal scan of Figure 3b. These topological ridges in Figure 3b are likely due to a thinner P3HT layer capping the crystal, allowing the ridges of the crystal to protrude the surface slightly. Notably, the ridge pattern on the crystal (Figure 3e) was more vivid but less frequent than the ridge pattern near the crystal (Figure 3c). The ridge pattern dichotomy is also observed in the optical photographs in Figure 1d, e when comparing the periodicity of the ridges on the centre of the crystals and around the edges.

The THz-TD measurements of the samples fabricated on glass and PVDF are plotted in Figure 4 with reference to a bare glass substrate. The P3HT:PCBM-PVDF sample was also measured with a glass substrate to ensure the consistency of the reference signal. The P3HT:PCBM samples delayed and attenuated the peak amplitude of the THz wave due to their relative complex refractive index $(\tilde{n} = n + i\kappa)$, such that

$$n = 1 + \frac{ct_s}{d}, and \kappa = \frac{c \ln\left(1 - A - A_0/A_0\right)}{4\pi df}$$
 (1)

where, A_o , A, and t_s are the amplitudes of the reference signal and sample signal, and the time delay, respectively. The sample thickness is defined as d while f and c are the frequency and speed of light in vacuum. The relative permittivity can be obtained by $\varepsilon_r = \tilde{n}^2$, assuming the relative permeability is close to unity based on the low magnetic response in Figure 2. The refractive index values and complex permittivity, averaging over three THz-TD measurements, are listed in Table 1. The real refractive index of the P3HT:PCBM fabricated on glass closely matches reported values in the literature [19,22], suggesting that the effect of the PCBM crystals on the photonic behaviour is marginal compared to amorphous films in this frequency range. The reduction in the refractive index for the P3HT:PCBM-PVDF sample is attributed to the inclusion of the PVDF substrate, where the refractive index for PVDF was previously reported to range from 1.4-2.1 in the THz region [23].

Traditional substrates, i.e., ITO-glass and bare glass, stipulate challenges for flexible, wearable, and biomedical electronics. Moreover, macroscale mechanical characterisation of P3HT:PCBM is experimentally challenging on these traditional substrates due to their overwhelming rigidity compared to the local modulus of P3HT:PCBM reported to be 550-600 MPa [23]. Thus, the mechanical properties of P3HT:PCBM-PVDF samples were characterised using a dynamic mechanical analyser (TA Q800) in uniaxial tension. Three P3HT:PCBM-PVDF samples were compared to pristine PVDF membranes, resulting in the averaged stressstrain behaviours in Figure 5. P3HT:PCBM decreased the strain-to-yield of the PVDF membrane by $65 \pm 0.3\%$, which is attributed to the chemical degradation from dichlorobenzene during processing. Nevertheless, the significant 24% maximum strain of P3HT:PCBM-PVDF is still suitable for compliant electronics.

The overall behaviour of the PVDF and P3HT:PCBM-PVDF samples bore little resemblance to any hyperelastic model for bulk polymers but did closely mimic the response of polymeric foam. This is attributed to the pore structure of

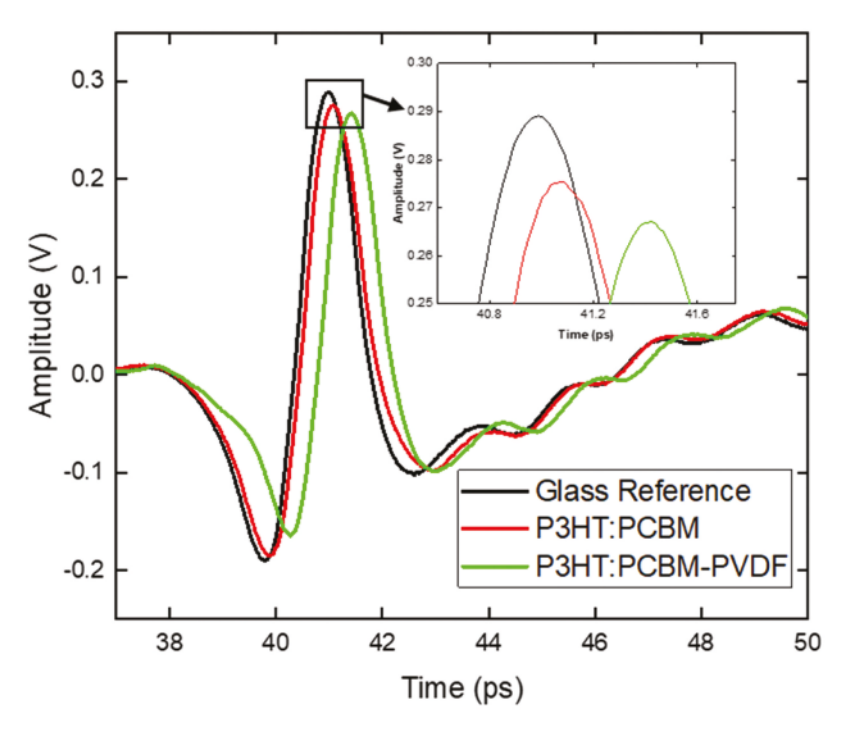


Figure 4. Terahertz time-domain signals of glass reference, P3HT:PCBM fabricated on glass, and P3HT:PCBM-PVDF samples.

Table 1. Optical and dielectric properties of P3HT:PCBM on glass and PVDF.

Sample	n	K	ϵ_r
P3HT:PCBM	3.30	2.6e-3	10.82 + 1.73i
P3HT:PCBM-PVDF	1.42	4.7e-4	2.00 + 0.15i

the PVDF membrane used here as the substrate (see SEM micrograph in the inset of Figure 5). Liu and Subhash proposed a phenomenological model [24] (referred to as the LS model herein) to describe the stress-strain relationship of polymeric foam under uniaxial tension, given as

$$\sigma = A \frac{e^{\alpha \varepsilon} - 1}{B + e^{\beta \varepsilon}} \tag{2}$$

where, σ and ε are the engineering stress and strain, respectively, A (units of stress), B, α , and β are curvefitting parameters [24]. Walter *et al.* explained that A is related to the stress of pore collapse and the ratio of the α and β parameters are related to material stiffening (if $\alpha/\beta > 1$) or softening (if $\alpha/\beta < 1$) [25]. The elastic modulus (E) can be obtained by differentiating Equation 2, $E = A\alpha/1 + B$.

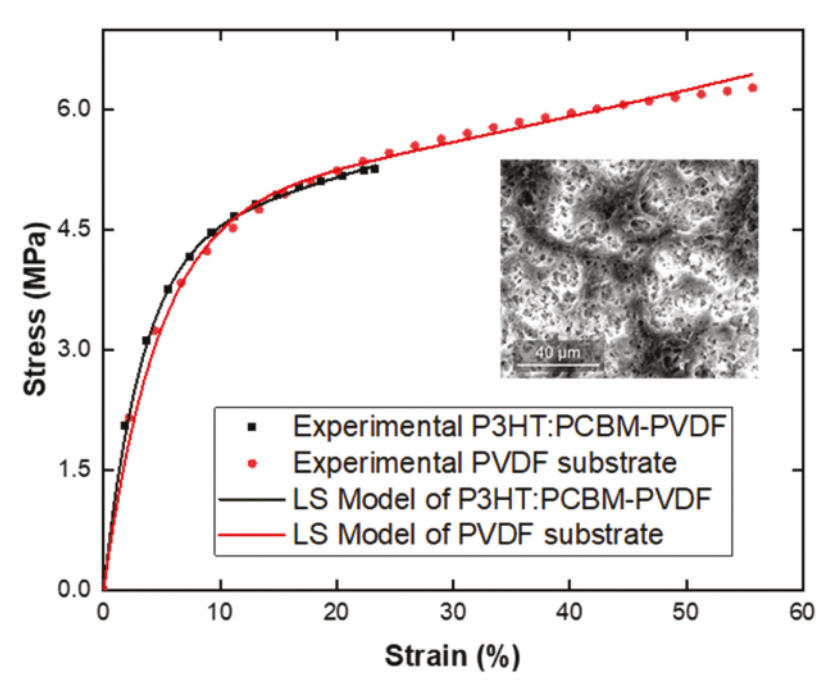


Figure 5. Engineering stress-strain of P3HT:PCBM-PVDF and PVDF substrate with their respective fitted Liu-Subhash model responses (the inset is an SEM micrograph of the porous structure of the PVDF substrate).

Table 2. Liu-subhash model parameters for PVDF substrate and P3HT:PCBM-PVDF.

Sample	A (MPa)	α	β	E (MPa)
P3HT:PCBM-PVDF	4.391 ± 0.014	0.306 ± 0.011	0.298 ± 0.011	1.344 ± 0.044
PVDF substrate	4.768 ±0.028	0.223±0.004	0.217±0.004	1.058±0.012

The mechanical properties extracted from the experimental stress-strain and the fitting parameters of the LS model are tabulated in Table 2. Overall, the LS model pronounces the effects of P3HT:PCBM on the mechanical response, including a 30% increase in stiffness and an 8% decrease in the pore collapse stress of the PVDF substrate. The 30% increase in stiffness is attributed to the higher rigidity of the PCBM crystals. Prior microscale characterisation reported that the PCBM crystals had a plane-stress stiffness of ~ 550 MPa, attributing its relatively high stiffness to the P3HT:PCBM-PVDF bulk. Thermogravimetric analysis revealed that P3HT:PCBM constituted ~9% of the weight of the tested P3HT:PCBM-PVDF samples. Moreover, image processing analysis showed that the PCBM crystals had an ~8% coverage of the sample surface. Using the in-plane force-balance relationship of laminate composites ($E_c a_c = E_1 a_1 + E_2 a_2$, where a is the cross-sectional area, and subscripts c, 1 and 2 represent the composite and the two constituents, respectively); the calculated stiffness of P3HT: PCBM is \sim 580 MPa, which is in excellent agreement with the prior microscale characterisation. Finally, the 8% decrease in pore collapse stress is attributed to P3HT:PCBM filling in the pores of PVDF.

In closing, this study reported synthesising colossal PCBM crystals on glass, ITO-coated glass, and PVDF substrates while overcoming detrimental polymer substrate challenges to the crystal growth process. When fabricating on glass, the PCBM crystals were found to seed directly on the substrate, while a layer of P3HT covered the crystals. The crystals had good adhesion to the glass and P3HT, causing failure when the P3HT separated. Conversely, when fabricated on PVDF, the uncoated P3HT was segregated from the PCBM crystals. The uncoated crystals revealed numerous features that P3HT previously occluded, but the separation was detrimental to the magnetic and conductive properties. When the phases were in contact (i.e., fabricated on glass), the colossal crystals outperformed the magnetic and conductive measurements of their amorphous counterparts reported a priori. The mechanical properties were also characterised and agreed with prior micromechanical measurements.

The research leading to these results was supported in part by the United States Department of Defense under Grant Agreement No. W911NF1410039 and W911NF1810477. The National Science Foundation under Award No. 1925539 also supported the research. The authors are also grateful for internal funding from San Diego State University. The authors also acknowledge the use of equipment at the San Diego State University Electron Microscopy Facility acquired by NSF instrumentation grant DBI-0959908.

Disclosure statement

No potential conflict of interest was reported by the author(s).

Funding

This work was supported by the Department of Defense; National Science Foundation [1925539].

ORCID

George Youssef http://orcid.org/0000-0003-2029-7692

Data availability statement

The data that support the findings of this study are available from the corresponding authors upon reasonable request.

References

- Ha S-T, Su R, Xing J, et al. Metal halide perovskite nanomaterials: synthesis and applications. Chem Sci. 2017;8(4):2522–2536. doi: 10.1039/C6SC04474C
- [2] Spaldin NA, Ramesh R. Advances in magnetoelectric multiferroics. Nat Mater. 2019;18(3):203-212. doi: 10.1038/ s41563-018-0275-2
- [3] Shekhah O, Liu J, Fischer R, et al. MOF thin films: existing and future applications. Chem Soc Rev. 2011;40(2):1081–1106. doi: 10.1039/c0cs00147c
- [4] Mhamdi A, ben Slama Sweii F, Saidi H, et al. Morphological, structural and optical properties of MEH-PPV: PC70BM nanocomposite film. J Mol Struct. 2018;1160:33–37. doi: 10.1016/j. molstruc.2018.01.063
- [5] Veenstra S, Verhees W, Kroon J, et al. Photovoltaic properties of a conjugated polymer blend of MDMO- PPV and PCNEPV. Chem Mater. 2004;16(12):2503-2508. doi: 10.1021/cm049917d
- [6] Berger P, Kim M. Polymer solar cells: P3HT:PCBM and beyond. J Renewable Sustain Energy. 2018;10(1). doi: 10. 1063/1.5012992
- [7] Dang MT, Hirsch L, Wantz G. P3HT:PCBM, best seller in polymer photovoltaic research. Wiley Online Library; 2011.
- [8] Vijay P, Sumaria V. Advancement in P3HT:PCBM solar cells, the most efficient polymer photovoltaic cell. 10th Annu Session Of Students' Chem Eng Congr (SCHEMCON). 2014;10:14.
- [9] Gobbi M, Orgiu E. The rise of organic magnetoresistance: materials and challenges. J Mater Chem C. 2017;5(23):5572–5580. doi: 10.1039/C6TC04403D
- [10] Ren S, Wuttig M. Organic exciton multiferroics. Adv Mater. 2012;24(6):724–727. doi: 10.1002/adma.201104250
- [11] Qin W, Jasion D, Chen X, et al. Charge-transfer magnetoelectrics of polymeric multiferroics. ACS Nano. 2014;8 (4):3671–3677. doi: 10.1021/nn500323j
- [12] Sitter H. Interface controlled organic thin films. In: Rubahn HG, Horowitz G, Al-Shamery K, editors. New York: Springer; 2009.
- [13] Yang B, Xiao Z, Yuan Y, et al. Room-temperature organic ferromagnetism in the crystalline poly (3-hexylthiophene): phenyl-C61-butyric acid methyl ester blend film. Polymer. 2013;54(2):490-494. doi: 10.1016/j.polymer.2012.12.024
- [14] Kaltenbrunner M, White MS, Głowacki ED, et al. Ultrathin and lightweight organic solar cells with high flexibility. Nat Commun. 2012;3(1):770. doi: 10.1038/ncomms1772
- [15] Yang Y, Liu C, Gao S, et al. Large [6, 6]-phenyl C61 butyric acid methyl (PCBM) hexagonal crystals grown by solvent-vapor annealing. Mater Chem Phys. 2014;145(3):327–333. doi: 10. 1016/j.matchemphys.2014.02.017
- [16] Bunshah RF. Handbook of deposition technologies for films and coatings: science, technology, and applications. Norwich, New York: William Andrew; 1994.
- [17] Mattox DM. Handbook of physical vapor deposition (PVD) processing. Burlington, MA: William Andrew; 2010.
- [18] Huynh N, Youssef G. Physical evidence of stress-induced conformational changes in polymers. Exp Mech. 2021;61 (3):469–481. doi: 10.1007/s11340-020-00673-7
- [19] Ulbricht R, Hendry E, Shan J, et al. Carrier dynamics in semiconductors studied with time-resolved terahertz



- spectroscopy. Rev Mod Phys. 2011;83(2):543. doi: 10.1103/RevModPhys.83.543
- [20] Shen S, Liu X, Shen Y, et al. Recent advances in the development of materials for terahertz metamaterial sensing. Adv Optical Mater. 2022;10(1):2101008. doi: 10.1002/adom.202101008
- [21] Farina M, Ye T, Lanzani G, et al. Fast ultrahigh-density writing of low-conductivity patterns on semiconducting polymers. Nat Commun. 2013;4(1):2668. doi: 10.1038/ncomms3668
- [22] Jeon T-I, Grischkowsky D, Mukherjee A, et al. Electrical and optical characterization of conducting poly-3-methylthiophene film by THz time-domain spectroscopy. Appl Phys Lett. 2001;79 (25):4142–4144. doi: 10.1063/1.1427754
- [23] Wang S, Wang S, Wang C, et al. Terahertz dielectric properties of polyvinylidene fluoride films. In: The International Photonics and Optoelectronics Meeting 2017, OSA Technical Digest. Optica Publishing Group; 2017 (online) (Optica Publishing Group, 2017). paper ASu3A.5.
- [24] Liu Q, Subhash G. A phenomenological constitutive model for foams under large deformations. Polym Eng Sci. 2004;44 (3):463–473. doi: 10.1002/pen.20041
- [25] Walter TR, Richards AW, Subhash G. A unified phenomenological model for tensile and compressive response of polymeric foams. J Eng Mater Technol. 2009;131(1). doi: 10.1115/ 1.3026556